Agricultural and Forest Meteorology 252 (2018) 231–240

Contents lists available at ScienceDirect

Agricultural and Forest Meteorology

journal homepage: www.elsevier.com/locate/agrformet

Variability and bias in active and passive ground-based measurements of effective plant, wood and leaf area index

Kim Calders[a,b,c,*], Niall Origo[a,b], Mathias Disney[b,d], Joanne Nightingale[a], William Woodgate[e], John Armston[f], Philip Lewis[b,d]

[a] Earth Observation, Climate and Optical Group, National Physical Laboratory, Teddington TW11 0LW, UK
[b] UCL Department of Geography, Gower Street, London WC1E 6BT, UK
[c] CAVElab – Computational & Applied Vegetation Ecology, Ghent University, Belgium
[d] NERC National Centre for Earth Observation (NCEO), UK
[e] Land and Water, Commonwealth Scientific and Industrial Research Organisation, Black Mountain, ACT, Australia
[f] Department of Geographical Sciences, University of Maryland, College Park, MD 20742, USA

ARTICLE INFO

Keywords:
Sensor comparison
Leaf area index
Terrestrial LiDAR
Hemispherical photography
LAI-2200
Validation

ABSTRACT

In situ leaf area index (LAI) measurements are essential to validate widely-used large-area or global LAI products derived, indirectly, from satellite observations. Here, we compare three common and emerging ground-based sensors for rapid LAI characterisation of large areas, namely digital hemispherical photography (DHP), two versions of a widely-used commercial LAI sensor (LiCOR LAI-2000 and 2200), and terrestrial laser scanning (TLS). The comparison is conducted during leaf-on and leaf-off conditions at an unprecedented sample size in a deciduous woodland canopy. The deviation between estimates of these three ground-based instruments yields differences greater than the 5% threshold goal set by the World Meteorological Organization. The variance at sample level is reduced when aggregated to plot scale (1 ha) or site scale (6 ha). TLS shows the lowest relative standard deviation in both leaf-on (11.78%) and leaf-off (13.02%) conditions. Whereas the relative standard deviation of effective plant area index (ePAI) derived from DHP relates closely to TLS in leaf-on conditions, it is as large as 28.14–29.74% for effective wood area index (eWAI) values in leaf-off conditions depending on the thresholding technique that was used. ePAI values of TLS and LAI-2x00 agree best in leaf-on conditions with a concordance correlation coefficient (CCC) of 0.796. In leaf-off conditions, eWAI values derived from DHP with Ridler and Calvard thresholding agrees best with TLS. Sample size analysis using Monte Carlo bootstrapping shows that TLS requires the fewest samples to achieve a precision better than 5% for the mean ± standard deviation. We therefore support earlier studies that suggest that TLS measurements are preferential to measurements from instruments that are dependent on specific illumination conditions. A key issue with validation of indirect estimates of LAI is that the true values are not known. Since we cannot know the true values of LAI, we cannot quantify the accuracy of the measurements. Our radiative transfer simulations show that ePAI estimates are, on average, 27% higher than eLAI estimates. Linear regression indicated a linear relationship between eLAI and ePAI–eWAI (R^2 = 0.87), with an intercept of 0.552 and suggests that caution is required when using LAI estimates.

1. Introduction

Leaf area index (LAI) is an essential climate variable (ECV) that describes the amount of leaf material in an ecosystem (Nemani et al., 2003; Asner et al., 2003; Disney et al., 2016). LAI is commonly used as a measurement of forest structure and its temporal patterns are used to monitor how biological cycles are connected and correspond to climate change (Polgar and Primack, 2011; White et al., 2009; Bequet et al., 2011; Calders et al., 2015b). To be useful for climate modelling, full end-to-end traceability and assessment of the uncertainty of the process from sensor measurement through to the generation of the ECV product and the resulting time-series is needed (Dowell et al., 2013). Space-borne estimates of LAI are essential to provide a greater spatial and temporal coverage compared to in situ estimates, but the retrieval process is more complex due to the mixed contributions of leaves, other tree elements, understorey vegetation and soil to the measured radiation flux. We require knowledge of the measurement uncertainty and the uncertainty of the derived ECV and its time-series. It is critical to

* Corresponding author at: CAVElab – Computational & Applied Vegetation Ecology, Ghent University, Belgium.
E-mail addresses: kim.calders@npl.co.uk, kim.calders@ugent.be (K. Calders).

https://doi.org/10.1016/j.agrformet.2018.01.029
Received 25 September 2017; Received in revised form 8 January 2018; Accepted 20 January 2018

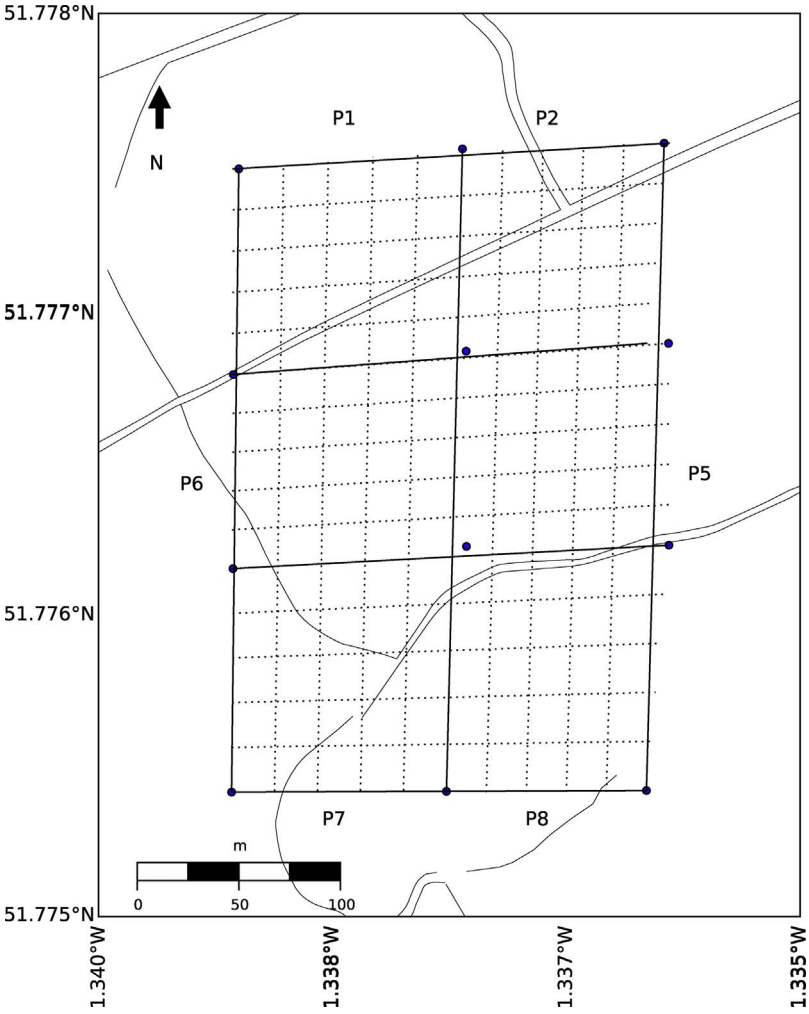

Fig. 1. The location of the 6 plots (1 ha) within the wider 6 ha study area. Figure modified from Origo et al. (2017).

benchmark the different (global) space-derived LAI products and compare these against in situ measurements to ensure their accuracy and reliability. The Global Climate Observing System (GCOS) specified the target requirements for LAI products to be a maximum of 15% uncertainty and 10% stability (the maximum acceptable change in systematic error per decade) (GCOS, 2016), with some target requirements being as low as 5% (WMO, 2012). WMO (2012) listed different breakthrough and threshold requirements depending on the application area of LAI products.

In situ observations are key for the validation of these global spaceborne LAI products. However, comparison of different in situ sensors demonstrated a level of variability typically above these targeted GCOS requirements (Ryu et al., 2010b; Woodgate et al., 2015b). These ground-based sensors measure light transmission and are therefore sensitive to all plant constituents (not just leaves), and plant area index (PAI) is therefore a more correct term. Ground-based sensors can essentially only measure PAI or WAI in deciduous forests, whereas LAI is the key input parameter for models related to climate, agricultural meteorology or hydrology (WMO, 2012). For clarity, within this paper we interpret LAI, PAI and WAI for broadleaved woody species as follows:

- **LAI** is half of the green leaf area per unit of horizontal ground surface area (Chen and Black, 1992).
- **PAI** is half of the surface area of all above-ground vegetation matter per unit of horizontal ground surface area.
- **WAI** is half of the surface area of all above-ground woody matter per unit of horizontal ground surface area.

Two of the most widely-used 2D ground-based passive instruments are digital hemispherical photography, DHP (Origo et al., 2017; Woodgate et al., 2015b) and the LAI-2000 or LAI-2200 (hereafter referred to as LAI-2x00) (Ryu et al., 2010a,b). Methodological errors can occur at any stage during data acquisition and analysis (Jonckheere et al., 2004). Measurement protocols for these instruments require specific light conditions and levelling, while analysis protocols generally involve image thresholding (DHP) and/or linking below and above canopy measurements to derive canopy gap fraction (LAI-2x00).

More recently, 3D terrestrial LiDAR (light detection and ranging) instruments are being used to estimate PAI and to quantify forest structure (Jupp et al., 2009; Calders et al., 2014; Vaccari et al., 2013; Cuni-Sanchez et al., 2016). Terrestrial LiDAR, also called terrestrial laser scanning (TLS), is an active remote sensing technique that accurately measures distances by transmitting laser pulses and analysing the returned energy as a function of distance or time (Newnham et al., 2015; Calders et al., 2015). TLS measurements are insensitive to light conditions and inclination sensors provide accurate instrument levelling information (Woodgate et al., 2015b).

This paper presents a direct comparison of effective PAI and WAI from three different sensors (DHP, LAI-2x00 and TLS) at the scale of medium-resolution satellite-products. Study areas in other comparisons of this sort are generally small, which hinders their ability to produce reliable comparison statistics that are representative of the wider vegetated area. For example, the number of sample points per study area in Woodgate et al. (2015b) ranged from 4 to 72, with a maximum plot area of 0.5 ha and only a few sample plots had coincident measurements of all three sensors. Ryu et al. (2010b) used a large study area,

covering 9 ha, but with only 47 coincident DHP and LAI-2000 sampling points i.e. approximately 5 sample points per ha. In this study we use 176 coincident DHP, LAI-2x00 and TLS measurements covering a 6 ha deciduous woodland site (i.e. approximately 30 sample points per ha). Measurements are collected in both leaf-on and leaf-off conditions, which allows us to better understand and quantify uncertainties related to PAI and WAI, and their sensitivity to leaf-presence. This large number of samples allows us to address issues of spatial variance and provide recommendations for more efficient use of current resources. We also present simulations of gap fraction using a Monte Carlo ray tracing (MCRT) radiative transfer model representation of a highly realistic 3D forest canopy. In this way, we can control all aspects of the crown structure, acquisition parameters and light conditions, which would not be possible using measured data. These simulations elucidate some of the more interesting relationships between PAI, WAI and LAI.

2. Materials and methods

2.1. Data collection and analysis

The study area was located within Wytham Woods, Oxford, UK and covered six ha of a larger 18 ha Smithsonian plot (Smithsonian Tropical Research Institute, 2016). The deciduous forest was dominated by Sycamore (*Acer pseudoplatanus*), Ash (*Fraxinus excelsior*) and Hazel (*Corylus avellana*) (Butt et al., 2009). The study area was divided into 6 × 1 ha plots (Fig. 1). Coincident data were collected at 176 locations within an approximate 20 m × 20 m grid (Held et al., 2015; Woodgate et al., 2012) covering the six ha study area. Some locations were sampled multiple times (two or four samples) with DHP and LAI-2x00 as part of a separate study and the gap fraction values for these different samples were averaged. Sensor data for this study were collected in leaf-on (June & July 2015) and leaf-off (December 2015 & January 2016) conditions. The sampling locations were marked with flags so sampling in both campaigns was done at the same locations. DHP images were collected in both field campaigns in a quasi-simultaneous fashion to the LAI-2x00 measurement to achieve similar illumination conditions (either overcast or after sunset).

The underlying theoretical principles that are used by different active and passive ground-based instruments are described in Appendix A. All these instruments correct for some of the clumping in different ways. Therefore, the comparison in this paper will focus on effective parameters (eLAI, ePAI, eWAI), which provides a like for like comparison.

Full details of the data analysis can be found in Appendix B. The LAI-2x00 and DHP methods calculate a single $P_{gap}(\theta)$ per measurement location and view zenith angle interval, whereas the TLS method also calculates a vertically resolved $P_{gap}(\theta, z)$ for each location and zenith angle interval. We compared two different automated DHP thresholding techniques: the global binary automated threshold method from Ridler and Calvard (1978) (DHP(G)) and two-corner classification procedure from Macfarlane et al. (2014) (DHP(TC)). We retrieved ePAI and eWAI by inverting the gap fraction model using a P_{gap} estimate of the hinge region in leaf-on and leaf-off conditions, respectively. The LAI-2x00 and DHP method used Eq. (A.2) and the TLS method used Eq. (B.4). The hinge region is generally used to approximate the 57.5° hinge angle (Jupp et al., 2009; Zhao et al., 2011; Calders et al., 2015b), where $G(\theta)$ is essentially invariant at 0.5 over different theoretical leaf and wood angle distributions (Ross, 1981; Woodgate et al., 2015a). This allows us to convert the gap fraction model without making assumptions about the foliage and wood orientation function. At the hinge angle the path length through the canopy to the top is about twice the canopy height, which implies significant spatial averaging is occurring (Jupp et al., 2009).

We used the *lm* function from the *stats* package in R (R Development Core Team, 2011) to implement a linear regression to compare estimates from the different ground-based sensors. We report the coefficient of determination, R^2, as well as the concordance correlation coefficient (CCC). The CCC computes the agreement on a continuous measure obtained by two methods (Lin, 1989) and ranges between −1 (perfect discordance) and 1 (perfect concordance).

2.2. Sampling experiment

Preliminary findings in Woodgate et al. (2012) suggested that measurements obtained using different sampling designs (grid, VALERI, SLATS) yielded comparable results. Here, we used a 20 m grid sampling (Wilkes et al., 2017) that resulted in 176 sample locations covering 6 ha or 36 locations per hectare. To optimise the use of resources, we analysed the effect of number of samples on the mean and standard deviation of the sampled unit. The analysis was done for the site (6 ha) and plot (1 ha) scale. For each sampling unit (site or plot), the global average and standard deviations were calculated from all data within the site or plot area. We employed a Monte Carlo bootstrapping procedure where a set number (in our case 1000) of random samples were removed for each sample number. For each permutation the absolute difference between the global and sample statistic was calculated.

2.3. Simulation experiment

We used the *librat* Monte Carlo ray tracing (MCRT) model to simulate gap fraction images (Lewis, 1999). This model has been tested in previous studies against other models (Widlowski et al., 2015, 2007; Pinty et al., 2004), as well as against observations (Disney et al., 2006, 2011; Calders et al., 2013; Woodgate et al., 2016). *Librat* estimates the radiative transfer regime within a canopy stochastically by following the interactions of sample rays propagating through a scene (i.e. a virtual forest) from sensor to source (Disney et al., 2000). This simulation environment enabled us to simulate ePAI, eLAI and eWAI from the same locations with exactly the same illumination conditions. We used the 1 ha Järvselja birch stand scene model, a canopy scene generated for the fourth phase of the radiative transfer model intercomparison (Widlowski et al., 2015). This 49 year old deciduous stand resembled the forest structure of Wytham Woods well, had a stem density of 1017 trees/ha and was dominated by birch, common Alder and aspen. A leaf-off version of the scene was generated by removing all of the leaves, while a leaves-only version was created by removing all of the woody components. Ten locations were chosen randomly throughout the scene, with the minimum distance between the sensor location and nearest tree being 0.5 m. Gap fraction was simulated directly (i.e. a black and white image) using an orthographic hemispherical lens approximating 5.5 megapixels at 1.5 m above the terrain. We retrieved ePAI, eLAI and eWAI by inverting the gap fraction model (Eq. (A.2)) using a P_{gap} estimate of the hinge region of 55–60° degree zenith.

3. Results

The individual measurements of gap fraction (P_{gap}) around the hinge angle are shown in Fig. 2a and b. The three different passive methods (LAI-2x00, DHP(G) & DHP(TC)) were benchmarked against the TLS measurements because the latter are insensitive to illumination conditions and inclination sensors provide accurate levelling. Fig. 2c and d show the corresponding ePAI and eWAI. In leaf-on conditions, the TLS and LAI-2x00 measurements agreed best (CCC = 0.796, and slope of 1.06), whereas the DHP values were consistently lower. In leaf-off conditions, we observed the best agreement between TLS and the DHP (G) method (CCC = 0.306). The strongest linear relationship was between the LAI-2x00 and TLS, however, there was a significant underestimation of LAI-2x00 values compared to the TLS (slope of 0.54).

Fig. 3 illustrates the spatial variation within the study area of the TLS values and the residuals for the passive methods. The leaf-on TLS P_{gap} value of 0.171 at coordinate $x = 160$, $y = 80$ resembles an outlier

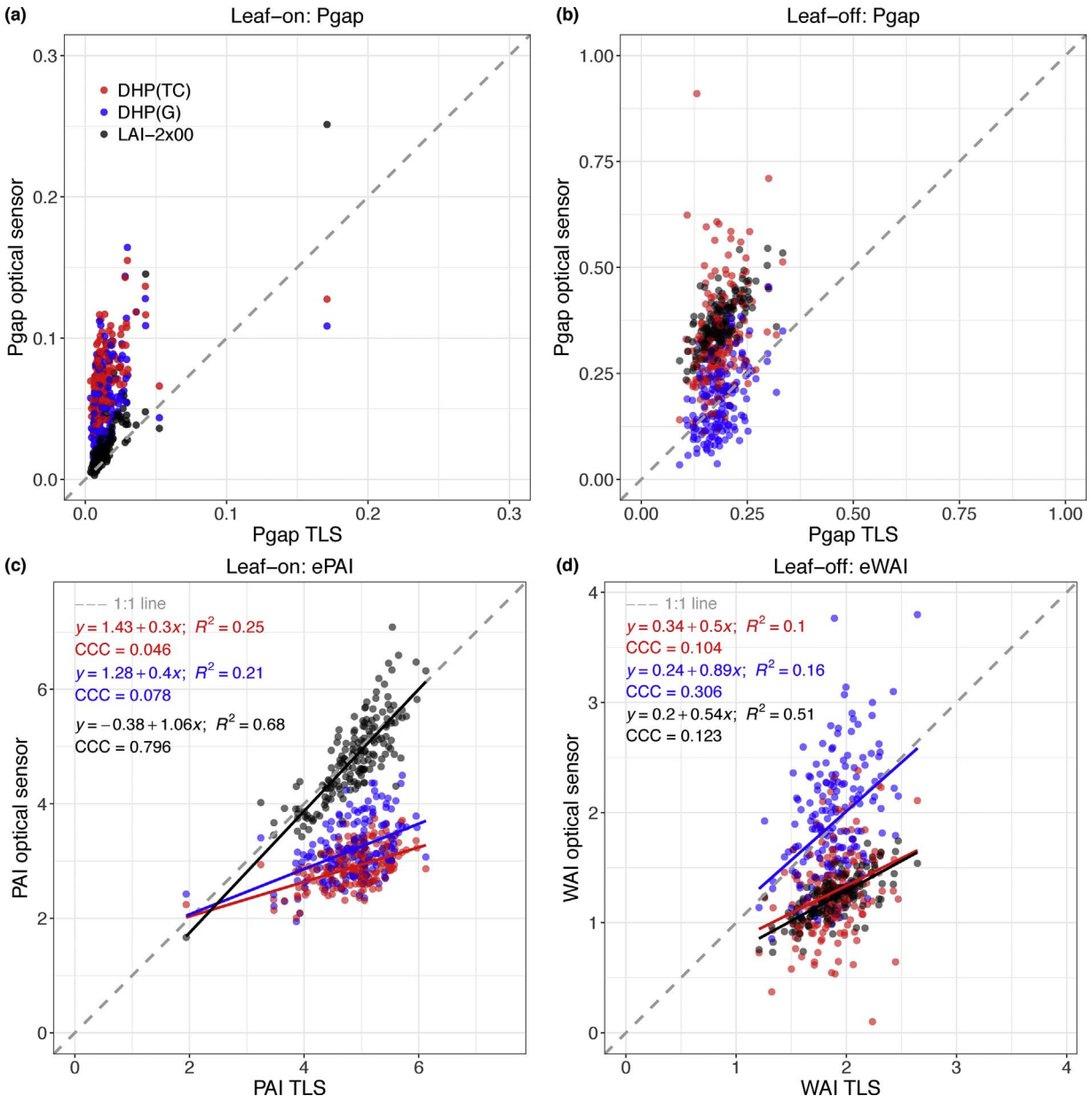

Fig. 2. Individual measurements for all 176 sample locations in leaf-on and leaf-off conditions. (a, b) Gap fraction around the hinge angle; (c, d) ePAI and eWAI.

but was actually caused by a clearing in the forest and registered by all instruments. Although Fig. 3 shows spatial variation in ePAI and eWAI, the mean plot and study area (site) values showed similar trends (Fig. 4). Similar to the individual measurements, the LAI-2x00 averages agreed best with TLS averages in leaf-on conditions, whereas DHP(G) estimates agreed best with TLS in leaf-off conditions. The relative ePAI standard deviation for the study area is similar for TLS (11.78%) and DHP(TC) (11.83%), followed by LAI-2x00 (15.38%) and DHP(G) (15.52%). In leaf-off conditions, the relative standard deviation around the study area average is 13.02% for TLS, 15.23% for LAI-2x00, 28.14% for DHP(G) and 29.74% for DHP(TC).

The large number of samples meant we could quantify the precision of each ground-based sensor using Monte Carlo bootstrapping (Fig. 5). The analysis for the different plots showed similar results and therefore we only showed results for plot P1 and the 6 ha study area. Table 1 summarises the number of samples required to achieve a precision of better than 5% for the mean ± standard deviation. Generally, a larger amount of samples was required to achieve the same precision for a larger area. The difference in required samples to achieve the same precision between leaf-on and leaf-off conditions was relatively small (ranging from 0 to 2) for TLS and LAI-2x00 but larger for both DHP methods. For example, the DHP(TC) method required 13 more samples for a 1 ha area (P1) and 39 more samples for the whole 6 ha study area in leaf-off conditions compared to leaf-on conditions.

Examples of simulated gap fraction images for the Järvselja birch stand scene model are shown in Fig. 6a. Simulations at 10 locations (Fig. 6b) showed that the average ePAI estimate (2.77 ± 0.44) was approximately 27% higher than the simulated eLAI values (2.18 ± 0.35). The average eLAI was approximately 43% higher than ePAI–eWAI (1.52 ± 0.31). The difference was largest for location F (64%) and smallest for location J (28%). Linear regression indicated a strong linear relationship between eLAI and ePAI–eWAI (R^2 = 0.87), with an intercept of 0.552.

4. Discussion

Within this paper, we compared three different ground-based instruments and quantified aspects of their measurement uncertainty.

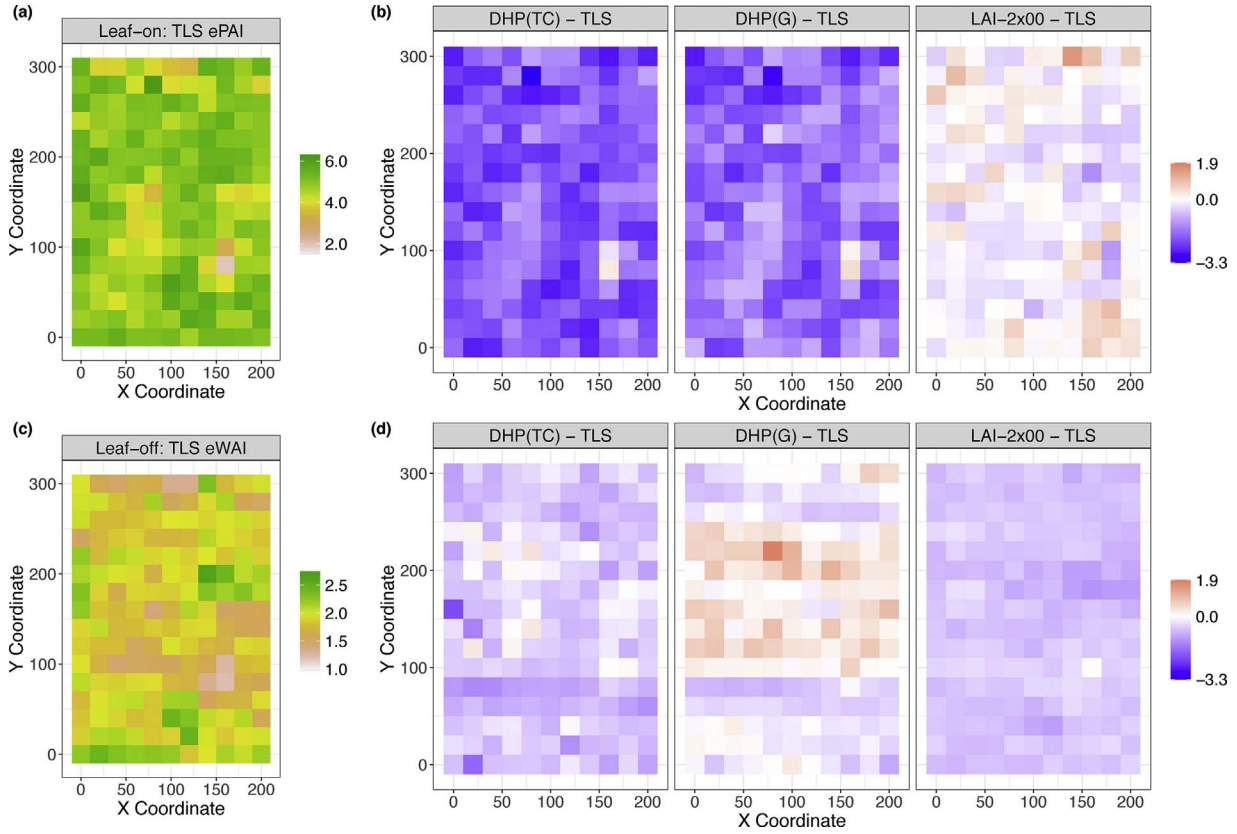

Fig. 3. Spatial maps of leaf-on ePAI and leaf-off eWAI. (a) Leaf-on ePAI estimates from TLS; (b) ePAI residuals of TLS vs. passive sensors; (c) Leaf-off eWAI estimates from TLS; (d) eWAI residuals of TLS vs. passive sensors.

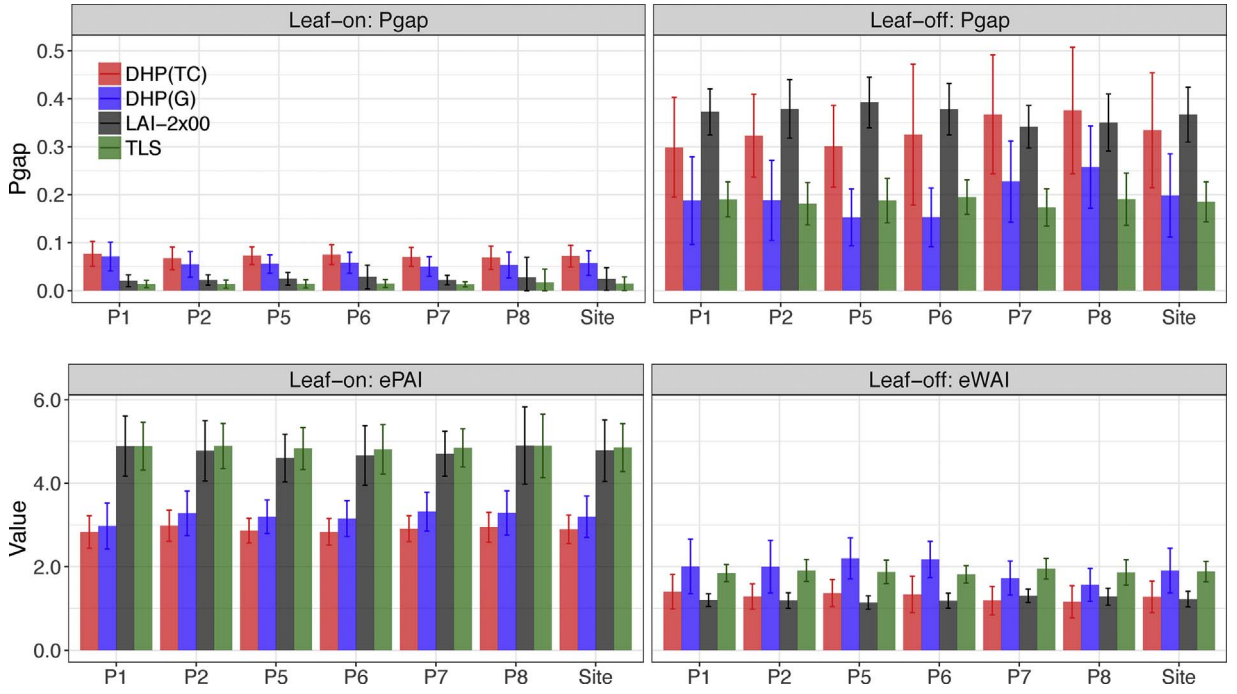

Fig. 4. Plot and study area (site) averages of gap fraction and leaf-on ePAI and leaf-off eWAI. The errorbars denote ± 1 standard deviation.

Similar to Woodgate et al. (2015b), Ryu et al. (2010b), our results indicated that the agreement between these instruments does not meet the 5% accuracy specified by WMO (2012). Ryu et al. (2010b) also reports higher estimates from LAI-2x00 measurements compared to DHP in savanna ecosystems. Woodgate et al. (2015b) compared the DHP(G) method against the DHP(TC) method for a range of Australian ecosystems. They found that PAI estimates were significantly different in three out of 11 sites, with DHP(G) resulting in a lower PAI compared to DHP(TC). We observed a larger ePAI for DHP(G) compared to DHP (TC) for the 6 ha study site ($p < 0.001$) and plots P2, P5, P6, P7, P8

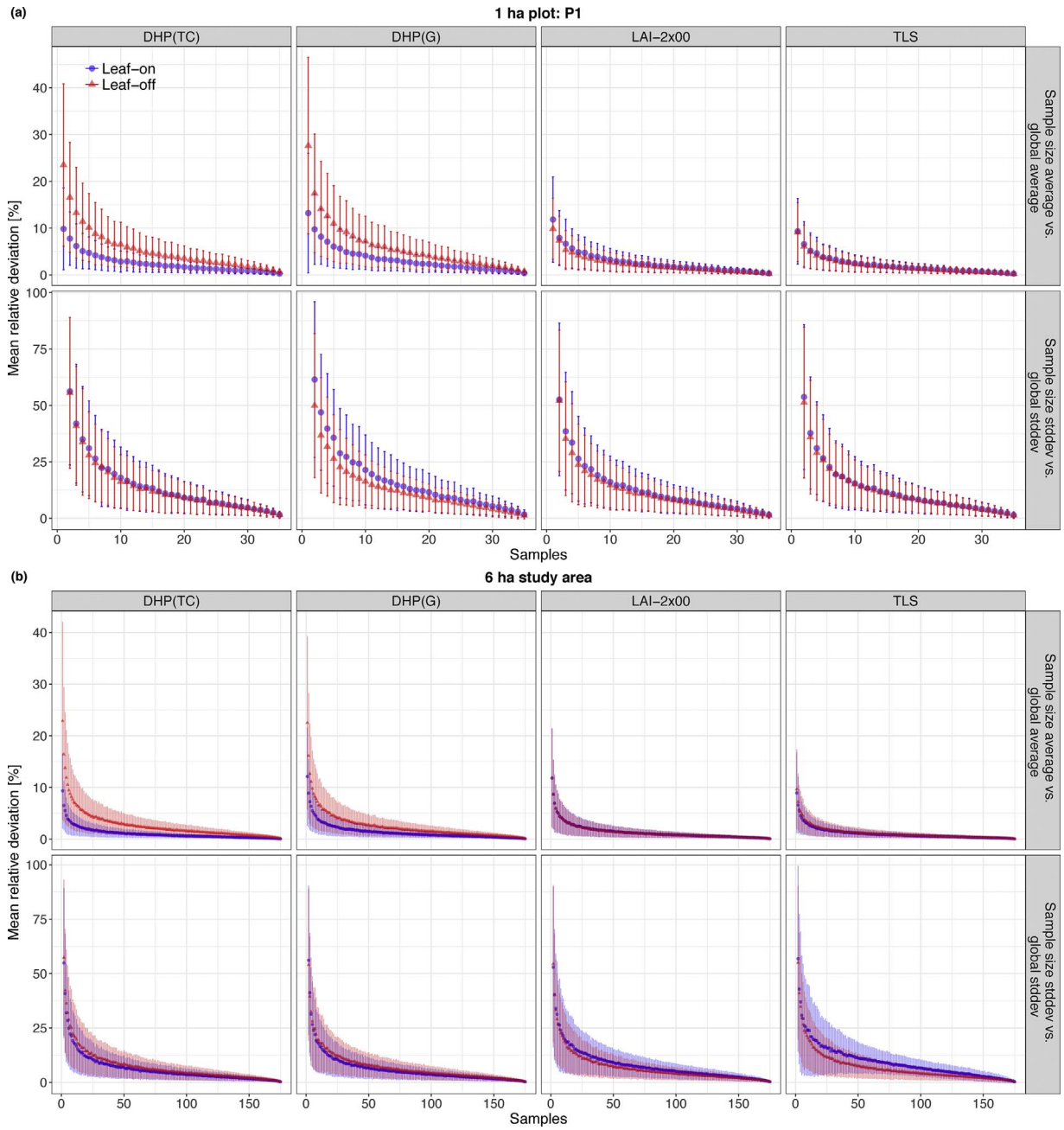

Fig. 5. Mean relative deviations of average and standard deviation (stddev) as a function of sample size. The errorbars denote ± 1 standard deviation. Only the study area and plot P1 data are shown here, the other five plots show similar behaviour.

Table 1
Number of samples required to achieve a precision of better than 5% for the mean ± standard deviation.

Plot (area)	Parameter	DHP(TC)	DHP(G)	LAI2x00	TLS
P1 (1 ha)	ePAI	11	15	12	9
	eWAI	24	25	10	8
Site (6 ha)	ePAI	11	17	17	11
	eWAI	50	47	17	13

($p < 0.01$), whereas there was no significant difference for P1. TLS ePAI estimates were largest, but not significantly different compared to LAI-2x00 for the study area and all plots. These larger values are because partial laser beam hits will always be classified as full hits, therefore underestimating the gap fraction. Two critical parameters in reducing the number of partial hits are the beam exit diameter and the beam divergence. The impact of partial hits in TLS data can be reduced by taking the intensity of the returns into account or by using full-waveform processing (if available) (Hancock et al., 2014; Jupp et al., 2009).

This study is unique as it presents a large number of coincident ePAI and eWAI measurements, whereas other studies had a much smaller sample size or only collected data in leaf-on conditions. The relative standard deviation was found to be smallest for TLS estimates in both leaf-off and leaf-on conditions, whereas this was variable for the other methods. The DHP(TC) relative standard deviation was comparable with TLS in leaf-on conditions, but more than doubled in leaf-off conditions. This might be due to more of the smaller plant constituents (e.g. twigs) being visible in leaf-off DHP images, resulting in more mixed pixels that are harder to classify. While hand-levelling resulted in similar results compared to tripod-levelling in leaf-on conditions (Origo

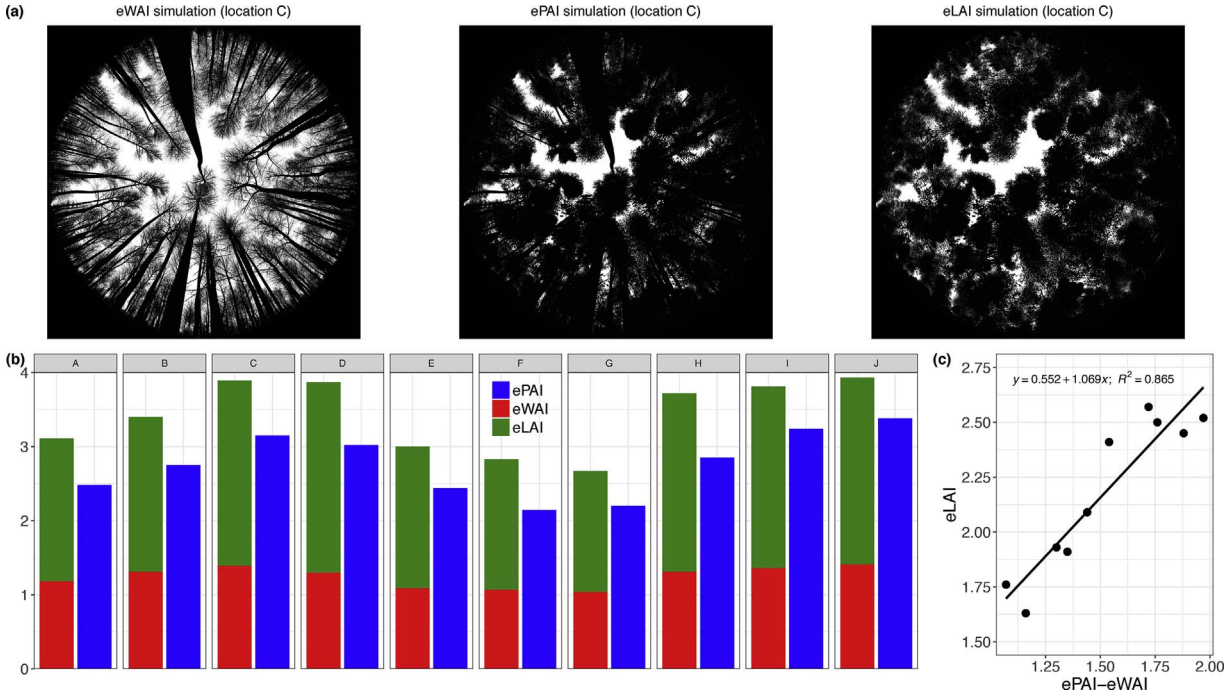

Fig. 6. (a) Example of simulated gap fraction images of eWAI, ePAI and eLAI for location C; (b) eWAI, eAI and eLAI values for 10 different locations; (c) linear regression of eLAI vs. ePAI minus eWAI.

et al., 2017), this has not been validated in leaf-off conditions and the combination of twigs and hand-levelling might result in more mixed pixels. However, hand-levelling can reduce the DHP acquisition time by a factor of eight and Fig. 5 demonstrates the importance of the number of samples on the mean relative deviation. Part of this deviation is due to the structural variation within the forest (Fig. 3) and part of this results from methodological errors during acquisition and analysis.

It is important to acknowledge that the variable that can be measured or inferred is often not the variable that is required in models. Earth system models provide feedback on climate change and rely on estimates of LAI to calculate, for example, stomatal conductance and photosynthesis (Friedlingstein et al., 2006). Small errors in LAI propagated through earth system models can become large errors in several biophysical and biogeochemical processes (Mahowald et al., 2016; Kala et al., 2014). Earth system models that use input from global spaceborne LAI products (e.g. MODIS) would therefore benefit from reliable ground validation for these products. The only approach to derive true LAI would be to destructively sample the leaves of trees. However, this is detrimental for the trees, highly impractical and time-consuming, and such measurements can therefore only be conducted on a very small scale. By relating gap fraction measurements from ground-based sensors to the variable of interest, these sensors provide a fast and non-destructive alternative to destructive sampling. However, these sensors are unable to estimate LAI and can only provide estimates of (effective) PAI (in leaf-on conditions) and WAI (in leaf-off conditions for deciduous forests). Our simulation results within a highly realistic 3D virtual birch stand demonstrated that, on average, the ePAI estimate was 27% higher than the eLAI estimate. These findings agree with Woodgate et al. (2016), who suggest a woody-to-total plant material estimate (α) to convert PAI to LAI. It is not surprising that the sum of individual eWAI and eLAI simulations is larger than the individual ePAI simulation. For a specific azimuth/zenith recording, Eq. (A.2) does not distinguish between single or multiple canopy elements on its path. When both leaf and wood elements are present in the simulated scene, the woody structure is preferentially obscured by the leafy crown shell. This interaction provides nonrandom occlusion that raises the gap probability and reduces the effective PAI.

The drawback of passive instruments is that gap probability estimates from image classification methods are very sensitive to illumination conditions. Hancock et al. (2014) found that manual thresholding DHPs by different operators resulted in a 17% range in gap fraction. They argued that TLS measurements should be preferred over passive measurements as they produce more stable estimates. Calders et al. (2015b) reported a relative standard deviation in eWAI from repeated leaf-off scans of 0.72% (including removing and setting up the tripod and instrument again over multiple days). Our results support the recommendation of favouring TLS over passive instruments. The lower TLS standard deviation results in fewer samples required for a similar area or a larger area to be sampled with similar resources, which would benefit the validation of global LAI products. The independence from illumination conditions and the availability of inclination sensors allows for more consistent and robust products. TLS not only provides an integrated canopy metric, but will also provide the vertically resolved plant area volume density or PAVD, which is a measure of the vertical plant material distribution through the canopy (Calders et al., 2014). Such additional information can significantly improve the phenology information provided to climate models that include phenology. Calders et al. (2017) demonstrated that the range accuracy of different same make and model TLS instruments was comparable and within the manufacturer's specification, which is essential for data interoperability. Other studies have compared different commercial and scientific TLS instruments (Armston et al., 2014; Newnham et al., 2012); highlighting differences between TLS instrument specification and configuration need to be considered in the estimation of (effective) PAI. The primary current disadvantage of TLS instruments is their purchase cost. However, recent developments have brought down the costs significantly and a range of low-cost TLS instruments is currently available, e.g. the Canopy Biomass LiDAR (Paynter et al., 2016), Leica BLK360 and FARO Focus^M 70. Since time-of-flight TLS instruments are independent of illumination conditions, the acquisition window is significantly larger than that of passive instruments. One could therefore argue that a TLS fieldwork day is more cost efficient, since more samples can be collected within the acquisition window. This has important implications for large area field campaigns where acquisition of

different sites under the same illuminations conditions is costly.

5. Conclusion

Our research demonstrates that caution is needed when using LAI estimates. The variable we measure with ground-based sensors is often (effective) PAI or WAI. Based on radiative transfer simulations, we show that average ePAI estimates are 27% higher than eLAI estimates. Linear regression indicated a strong linear relationship between eLAI and ePAI–eWAI ($R^2 = 0.87$). Based on our comparison of three different ground-based sensors, we recommend the use of TLS to provide a more stable estimate of gap fraction and to derive ePAI or eWAI. TLS generally requires fewer measurements to capture the spatial variability than the passive methods tested within this study. The independence from illumination conditions means that TLS provides more stable spatial estimates in leaf-on and leaf-off conditions and enabled a larger measurement acquisition window, which translates to more efficient fieldwork.

Acknowledgements

The research leading to these results was funded through the Metrology for Earth Observation and Climate project (MetEOC-2), grant number ENV55 within the European Metrology Research Programme (EMRP). The EMRP is jointly funded by the EMRP participating countries within EURAMET and the European Union. Funds for purchase of the UCL RIEGL VZ-400 instrument was provided by the UK NERC National Centre for Earth Observation (NCEO). We thank A. Barker, T. Jackson, S. Moorthy, P. Wilkes, M. Boni Vicari and D. Fox for their assistance with fieldwork and C. Macfarlane for providing the DCP processing software. The authors would like to thank N. Fisher and Y. Malhi for their support and for allowing us to use Wytham Woods for this study.

Appendix A. Theoretical background

The principles of light extinction in plant canopies was first described by Masami and Toshiro (1953) using a Poisson distribution and followed the common form of the Beer–Lambert law:

$$P_{\text{gap}}(\theta) = e^{-G(\theta)\text{LAI}/\cos(\theta)} \tag{A.1}$$

$P_{gap}(\theta)$ is the canopy gap probability from the ground, looking upward at view zenith angle θ and LAI is the leaf area index. $G(\theta)$ is the foliage orientation function and equals the projection of a unit area of foliage on a plane perpendicular to the direction θ, averaged over elements of all orientations (Ross, 1981). Eq. (A.1) describes the case of randomly dispersed canopy constituents. Nilson (1971) used a Markov model to account for non-random spatial distribution of leaves and introduced the clumping index, Ω:

$$P_{\text{gap}}(\theta) = e^{-G(\theta)\Omega\text{LAI}/\cos(\theta)} = e^{-G(\theta)\text{eLAI}/\cos(\theta)} \tag{A.2}$$

Ω describes the degree of dependence of the positions of leaves in neighbouring layers and $\Omega < 1$ is clumped and as Ω approaches 1, the canopy becomes more homogeneous until $\Omega = 1$, which essentially means a random distribution of leaves. eLAI is the effective leaf area index and is defined as $\Omega \times$ LAI. It is still difficult to quantify Ω from field measurements (Woodgate et al., 2017), which limits our understanding of clumping. Clumping occurs at multiple scales within the canopy: shoot level, between-crown level and ecosystem level (Ryu et al., 2010a).

Appendix B. Data processing

B.1 LAI-2x00

The LAI-2x00 instrument (LI-COR Inc., Lincoln, Nebraska USA) measures radiation received by a fish-eye optical sensor in five zenith rings with $\overline{\theta}$ being 7°, 23°, 38°, 53° and 68°. $\overline{\theta}$ is defined as the mid-point of the finite zenith angle interval used to aggregate measurements from different azimuth angles. The instrument filters wavelengths above 490 nm to retain a blue band in which the contrast between vegetation and sky is maximal (Zhao et al., 2011). P_{gap} was derived from a pair of measurements, as per the LI-COR manual; one related to the radiation under a forest canopy (B) and comparing them to measurements of skylight collected simultaneously in a nearby open area (A):

$$P_{\text{gap},i}(\overline{\theta_i}) = \frac{B_i}{A_i} \tag{B.1}$$

where subscript i refers to an optical sensor zenith ring ($i = 1, \ldots, 5$). The fourth ring ranges from 47.3° to 58.1° and was used to approximate the hinge region. The effective plant and wood area index was calculated using Eq. (A.2).

We used two instruments to collect near-simultaneous below and above canopy readings. A LAI-2000 instrument was set up in a nearby open area, approximately 600 m from the study area, to collect above canopy readings autonomously every 30 s. Four below canopy measurements were taken and averaged for each location with a LAI-2200 instrument. Both instruments had a 90° view cap, oriented towards the South. The instruments were used at a height of approximately 1.3 m, with the sensor oriented North so the operator was excluded from the field of view. The measurements were paired to calculate P_{gap} (Eq. (B.1)), matching the times of the individual measurements as closely as possible. The LAI-2000 and its successor, the LAI-2200, are designed to produce the same results (LI-COR Inc., 2011). We calibrated both instruments against each other using multiple datasets of simultaneous and co-located measurements. Robust linear regression (*rlm* function from the MASS package (Venables and Ripley, 2002) in R (R Development Core Team, 2011) was used for each ring individually. We performed separate calibrations for each measurement campaign to better match the dynamic range of values for each campaign.

B.2 Digital hemispherical photography

Images were captured using a Canon 5D full-frame DSLR with Sigma 8 mm fisheye lens which has a nominal field of view of 180°. The camera settings were selected based on recommendations from the literature (Woodgate et al., 2015b; Promis et al., 2011; Pueschel et al., 2012; Chianucci and Cutini, 2012; Glatthorn and Beckschäfer, 2014). The camera was set to record automatic exposure in high quality JPEG and RAW format. The camera was levelled at each location using the hand-levelling procedure described in Origo et al. (2017), and it was also ensured that field conditions

(such as wind speed and non-uniform background illumination) did not exceed acceptable thresholds based on the literature. Origo et al. (2017) reported that the average difference between tripod-levelling and hand-levelling for this study area was < 2% for effective plant area index. More importantly, hand-levelling can be up to eight times faster compared to tripod levelling, which is essential for sampling larger areas and providing validation support to global products at satellite scales.

We converted the RAW image file to jpeg using the open source software functionality of dcraw (www.cybercom.net/~dcoffin/dcraw/) in order to avoid the post-processing implemented by the camera software (Macfarlane et al., 2014). Only the blue channel of the image was included for the analysis in the Hemisphere software (Schleppi and Conedera, 2007) and the pre-loaded Sigma 8 mm lens calibration function was used in the processing. Post-processing of DHP images converted sensor brightness values to gap fraction within pre-specified regions of the image (cells or rings) by taking the ratio of the number of pixels defined as gap (*nG*) to the total number of pixels illuminated by the scene (*nT*):

$$P_{\text{gap},i}(\overline{\theta_i}) = \frac{\text{nG}_i}{\text{nT}_i} \tag{B.2}$$

The classification of pixels as gap or non-gap was done by thresholding the RGB image into a black (non-gap, $nT_i - nG_i$) and white (gap, nG_i) image (Woodgate et al., 2015b; Thimonier and Sedivy, 2010; Weiss et al., 2004). We retrieved ePAI and eWAI by inverting the gap fraction model (Eq. (A.2)) using a P_{gap} estimate of the hinge region of 55–60° degree zenith, in leaf-on and leaf-off conditions, respectively.

We compared two different automated thresholding techniques: the global binary automated threshold method from Ridler and Calvard (1978) (DHP(G)) and two-corner classification procedure from Macfarlane et al. (2014) (DHP(TC)). The DHP(G) uses iterative clustering to determine the optimal threshold through determination of the mean of the two cluster means. Jonckheere et al. (2005) found that from a selection of methods the method from Ridler and Calvard (1978) provided the most robust threshold values for a wide range of light and canopy structure conditions. The DHP(TC) method identifies unambiguous canopy and sky peaks in the image histogram and then detected the two corners at the point of maximum curvature. Mixed pixels are subsequently classified with the dual binary threshold (Macfarlane, 2011).

B.3 Terrestrial LiDAR

Terrestrial LiDAR data were acquired with a RIEGL VZ-400 terrestrial laser scanner (RIEGL Laser Measurement Systems GmbH). The instrument has a beam divergence of nominally 0.35 mrad and operates in the infrared (wavelength 1550 nm) with a range up to 350 m. The pulse repetition rate at each scan location was 300 kHz, the minimum range was 0.5 m and the angular sampling resolution was 0.04°.

Newnham et al., (2012); Lovell et al., (2011); Calders et al., (2014, 2015b) approximated the vertically resolved directional gap probability from a single terrestrial LiDAR scan as:

$$P_{\text{gap}}(\overline{\theta_i}, z) = 1 - \frac{\sum w_j(z_j < z, \overline{\theta_i})}{N(\overline{\theta_i})}$$
$$w = 1/n_s \tag{B.3}$$

where z is the height above terrain, the numerator in Eq. (B.3) gives the number of laser returns that are below z and $N(\overline{\theta_i})$ is the total number of outgoing laser pulses for the zenith angle interval. n_s is the number of total returns for that transmitted laser pulse and we make the assumption that for a specific transmitted laser pulse, each return represents a beam area interception of $1/n_s$.

Jupp et al. (2009) introduced a linear model to estimate vertically resolved eLAI at the hinge region as follows:

$$\text{eLAI}(z) = -1.1 \times \ln(P_{\text{gap}}(\overline{\theta_h}, z)) \tag{B.4}$$

The effective total LAI is equal to $L_e(z = z_{max})$, where z_{max} is the height of the canopy. The zenith ring between 55° and 60° was used to approximate the hinge region $\overline{\theta_h}$ (Jupp et al., 2009; Zhao et al., 2011; Calders et al., 2015b). The TLS data were processed in the open source python library *pylidar* that implemented the above methods (www.pylidar.org).

References

Armston, J., Newnham, G., Strahler, A., Schaaf, C., Danson, M., et al., 2014. A comparison of terrestrial laser scanning instruments for assessing forested ecosystems. In: ForestSAT 2014. 4–7 November 2014, Riva del Garda, Italy.

Asner, G.P., Scurlock, J.M.O., Hicke, A.J., 2003. Global synthesis of leaf area index observations: implications for ecological and remote sensing studies. Glob. Ecol. Biogeogr 12, 191–205.

Bequet, R., Campioli, M., Kint, V., Vansteenkiste, D., Muys, B., Ceulemans, R., 2011. Leaf area index development in temperate oak and beech forests is driven by stand characteristics and weather conditions. Trees Struct. Funct. 25, 935–946.

Butt, N., Campbell, G., Malhi, Y., Morecroft, M., Fenn, K., Thomas, M., 2009. Initial Results From Establishment of a Long-Term Broadleaf Monitoring Plot at Wytham Woods. University of Oxford, Oxford, UK.

Calders, K., Lewis, P., Disney, M., Verbesselt, J., Herold, M., 2013. Investigating assumptions of crown archetypes for modelling LiDAR returns. Remote Sens. Environ. 134, 39–49.

Calders, K., Armston, J., Newnham, G., Herold, M., Goodwin, N., 2014. Implications of sensor configuration and topography on vertical plant profiles derived from terrestrial LiDAR. Agric. For. Meteorol. 194, 104–117.

Calders, K., Newnham, G., Burt, A., Murphy, S., Raumonen, P., Herold, M., Culvenor, D., Avitabile, V., Disney, M., Armston, J., Kaasalainen, M., 2015. Nondestructive estimates of above-ground biomass using terrestrial laser scanning. Methods Ecol. Evol. 6, 198–208.

Calders, K., Schenkels, T., Bartholomeus, H., Armston, J., Verbesselt, J., Herold, M., 2015b. Monitoring spring phenology with high temporal resolution terrestrial lidar measurements. Agric. For. Meteorol. 203, 158–168.

Calders, K., Disney, M.I., Armston, J., Burt, A., Brede, B., Origo, N., Muir, J., Nightingale, J., 2017. Evaluation of the range accuracy and the radiometric calibration of multiple terrestrial laser scanning instruments for data interoperability. IEEE Trans. Geosci. Remote Sens. 55, 2716–2724.

Chen, J., Black, T., 1992. Defining leaf area index for non-flat leaves. Plant Cell Environ. 15, 421–429.

Chianucci, F., Cutini, A., 2012. Digital hemispherical photography for estimating forest canopy properties: current controversies and opportunities. IForest 5, 290–295.

Cuni-Sanchez, A., White, L.J.T., Jeffrey, K.J., Calders, K., Burt, A., Disney, M., Gilpin, M., Lewis, S.L., 2016. African savanna-forest boundary dynamics: a 20-year study. PLOS ONE 11, e0156934.

Disney, M.I., Lewis, P., North, P.R.J., 2000. Monte Carlo ray tracing in optical canopy reflectance modelling. Remote Sens. Rev. 18, 163–196.

Disney, M., Lewis, P., Saich, P., 2006. 3D modelling of forest canopy structure for remote sensing simulations in the optical and microwave domains. Remote Sens. Environ. 100, 114–132.

Disney, M., Lewis, P., Gomez-Dans, J., Roy, D., Wooster, M.J., Lajas, D., 2011. 3D radiative transfer modelling of fire impacts on a two-layer savanna system. Remote Sens. Environ. 115, 1866–1881.

Disney, M., Muller, J.P., Kharbouche, S., Kaminski, T., Vobeck, M., Lewis, P., Pinty, B., 2016. A new global fAPAR and LAI dataset derived from optimal albedo estimates: comparison with MODIS products. Remote Sens. 8, 275.

Dowell, M., Lecomte, P., Husband, R., Schulz, J., Mohr, T., Tahara, Y., Eckman, R., Lindstrom, E., Wooldridge, C., Hilding, S., Bates, J., Ryan, B., Lafeuille, J., Bojinski, S., 2013. Strategy Towards an Architecture for Climate Monitoring from Space. Available on http://www.wmo.int/pages/prog/sat/documents/ARCH_strategy-climate-architecture-space.pdf.

Friedlingstein, P., Cox, P., Betts, R., Bopp, L., von Bloh, W., Brovkin, V., Cadule, P.,

Doney, S., Eby, M., Fung, I., Bala, G., John, J., Jones, C., Joos, F., Kato, T., Kawamiya, M., Knorr, W., Lindsay, K., Matthews, H., Raddatz, T., Rayner, P., Reick, C., Roeckner, E., Schnitzler, K.G., Schnur, R., Strassmann, K., Weaver, A., Yoshikawa, C., Zeng, N., 2006. Climate-carbon cycle feedback analysis: results from the C4MIP model intercomparison. Geosci. Model Dev. 19, 3337–3353.

GCOS, 2016. The Global Observing System for Climate: Implementation Needs. Available on https://public.wmo.int/.

Glatthorn, J., Beckschäfer, P., 2014. Standardizing the protocol for hemispherical photographs: accuracy assessment of binarization algorithms. PLOS ONE 9, e111924.

Hancock, S., Essery, R., Reid, T., Carle, J., Baxter, R., Rutter, N., Huntley, B., 2014. Characterising forest gap fraction with terrestrial LiDAR and photography: an examination of relative limitations. Agric. For. Meteorol. 189–190, 105–114.

Held, A., Phinn, S., Soto-Berelov, M., Jones, S., 2015. AusCover Good Practice Guidelines: a technical handbook supporting calibration and validation activities of remotely sensed data products, version 1.1. TERN AusCover 352.

Jonckheere, I., Fleck, S., Nackaerts, K., Muys, B., Coppin, P., Weiss, M., Baret, F., 2004. Review of methods for in situ leaf area index determination. Part I. Theories, sensors and hemispherical photography. Agric. For. Meteorol. 121, 19–35.

Jonckheere, I., Nackaerts, K., Muys, B., Coppin, P., 2005. Assessment of automatic gap fraction estimation of forests from digital hemispherical photography. Agric. For. Meteorol. 132, 96–114.

Jupp, D.L.B., Culvenor, D.S., Lovell, J.L., Newnham, G.J., Strahler, A.H., Woodcock, C.E., 2009. Estimating forest LAI profiles and structural parameters using a ground-based laser called Echidna®. Tree Physiol. 29, 171–181.

Kala, J., Decker, M., Exbrayat, J.F., Pitman, A., Carouge, C., Evans, J., Abramowitz, G., Mocko, D., 2014. Influence of leaf area index prescriptions on simulations of heat, moisture, and carbon fluxes. J. Hydrometeorol. 15, 489–503.

Lewis, P., 1999. Three-dimensional plant modelling for remote sensing simulation studies using the Botanical Plant Modelling System. Agron. Agric. Environ. 19, 185–210.

LI-COR Inc, 2011. LAI-2200 Plant Canopy Analyzer Instruction Manual.

Lin, L., 1989. A concordance correlation coefficient to evaluate reproducibility. Biometrics 45, 255–268.

Lovell, J.L., Jupp, D.L.B., van Gorsel, E., Jimenez-Berni, J., Hopkinson, C., Chasmer, L., 2011. Foliage profiles from ground based waveform and discrete point lidar. In: SilviLaser 2011. 16–20 October 2011, Hobart, Australia.

Macfarlane, C., Ryu, Y., Ogden, G., Sonnentag, O., 2014. Digital canopy photography, exposed and in the raw. Agric. For. Meteorol. 197, 244–253.

Macfarlane, C., 2011. Classification method of mixed pixels does not affect canopy metrics from digital images of forest overstorey. Agric. For. Meteorol. 151, 833–840.

Mahowald, N., Lo, F., Zheng, Y., Harrison, L., Funk, C., Lombardozzi, D., Goodale, C., 2016. Projections of leaf area index in earth system models. Earth Syst. Dyn. 7, 211–229.

Masami, M., Toshiro, S., 1953. Über den lichtfaktor in den pflanzengesellschaften und seine bedeutung für die stoffproduktion. Jpn. J. Bot. 14, 22–52.

Nemani, R.R., Keeling, C.D., Hashimoto, H., Jolly, W.M., Piper, S.C., Tucker, C.J., Myneni, R.B., Running, S.W., 2003. Climate-driven increases in global terrestrial net primary production from 1982 to 1999. Science 300, 1560–1563.

Newnham, G., Armston, J., Muir, J., Goodwin, N., Tindall, D., Culvenor, D., Püschel, P., Nyström, M., Johansen, K., 2012. Evaluation of terrestrial laser scanners for measuring vegetation structure. CSIRO Sustain. Agric. Flagship. Available on https://publications.csiro.au/rpr/pub?pid=csiro:EP124571.

Newnham, G., Armston, J., Calders, K., Disney, M., Lovell, J., Schaaf, C., Strahler, A., Danson, F., 2015. Terrestrial laser scanning for plot scale forest measurement. Curr. For. Rep. 1, 239–251.

Nilson, T., 1971. A theoretical analysis of the frequency of gaps in plant stands. Agric. Meteorol. 8, 25–38.

Origo, N., Calders, K., Nightingale, J., Disney, M., 2017. Influence of levelling technique on the retrieval of canopy structural parameters from digital hemispherical photography. Agric. For. Meteorol. 237–238, 143–149.

Paynter, I., Saenz, E., Genest, D., Peri, F., Erb, A., Li, Z., Wiggin, K., Muir, J., Raumonen, P., Schaaf, E.S., Strahler, A., Schaaf, C., 2016. Observing ecosystems with lightweight, rapid-scanning terrestrial lidar scanners. Remote Sens. Ecol. Conserv. 2, 174–189.

Pinty, B., Widlowski, J.L., Taberner, M., Gobron, N., Verstraete, M.M., Disney, M., Gascon, F., Gastellu, J.P., Jiang, L., Kuusk, A., Lewis, P., Li, X., Ni-Meister, W., Nilson, T., North, P., et al., 2004. Radiation transfer model intercomparison (RAMI) exercise: results from the second phase. J. Geophys. Res. 109, D06210.

Polgar, C., Primack, R., 2011. Leaf-out phenology of temperate woody plants: from trees to ecosystems. N. Phytol. 191, 926–941.

Promis, A., Gärtner, S., Butler-Manning, D., Durán-Rangel, C., Reif, A., Cruz, G., Hernández, L., 2011. Comparison of four different programs for the analysis of hemispherical photographs using parameters of canopy structure and solar radiation transmittance. Waldokol. Online 11, 19–33.

Pueschel, P., Buddenbaum, H., Hill, J., 2012. An efficient approach to standardizing the processing of hemispherical images for the estimation of forest structural attributes. Agric. For. Meteorol. 160, 1–13.

R Development Core Team, 2011. R: A Language and Environment for Statistical Computing. R Foundation for Statistical Computing, Vienna, Austria ISBN: 3-900051-07-0.

Ridler, T.W., Calvard, S., 1978. Picture thresholding using an iterative selection method. IEEE Syst. Man Cybern. Mag. 8, 630–632.

Ross, J., 1981. The Radiation Regime and Architecture of Plant Stands. W. Junk Publishers, The Hague, pp. 391.

Ryu, Y., Nilson, T., Kobayashi, H., Sonnentag, O., Law, B.E., Baldocchi, D.D., 2010a. On the correct estimation of effective leaf area index: does it reveal information on clumping effects? Agric. For. Meteorol. 150, 463–472.

Ryu, Y., Sonnentag, O., Nilson, T., Vargas, R., Kobayashi, H., Wenk, R., Baldocchi, D.D., 2010b. How to quantify tree leaf area index in an open savanna ecosystem: a multi-instrument and multi-model approach. Agric. For. Meteorol 150, 63–76.

Schleppi, P., Conedera, M.S.I.T.A., 2007. Correcting non-linearity and slope effects in the estimation of the leaf area index of forests from hemispherical photographs. Agric. For. Meteorol. 144, 236–242.

Smithsonian Tropical Research Institute, 2016. Plots Summary. Available at http://www.ctfs.si.edu/plots/summary/.

Thimonier, A., Sedivy, I.P.S., 2010. Estimating leaf area index in different types of mature forest stands in Switzerland: a comparison of methods. Eur. J. For. Res. 129, 543–562.

Vaccari, S., van Leeuwen, M., Calders, K., Coops, N.C., Herold, M., 2013. Bias in LiDAR-based canopy gap fraction estimates. Remote Sens. Lett. 4, 391–399.

Venables, W.N., Ripley, B.D., 2002. Modern Applied Statistics with S-PLUS, 4th ed. Springer, New York ISBN 0-387-95457-0.

Weiss, M., Baret, F., Smith, G., Jonckheere, I., Coppin, P., 2004. Review of methods for in situ leaf area index (LAI) determination – Part II. Estimation of LAI, errors and sampling. Agric. For. Meteorol. 121, 37–53.

White, M.A., de Beurs, K.M., Didan, K., Inouye, D.W., Richardson, A.D., Jensen, O.P., O'Keefe, J., Zhang, G., Nemani, R.R., van Leeuwen, W.J.D., Brown, J.F., de Wit, A., Schaepman, M., Lin, X., Dettinger, M., et al., 2009. Intercomparison, interpretation, and assessment of spring phenology in North America estimated from remote sensing for 1982–2006. Glob. Change Biol. 15, 2335–2359.

Widlowski, J.L., Taberner, M., Pinty, B., Bruniquel-Pinel, D., Disney, M., Fernandes, R., Gastellu-Etchegorry, J.P., Gobron, N., Kuusk, A., Lavergne, T., Leblanc, S., Lewis, P.E., Martin, E., Möttus, M., North, P.R.J., et al., 2007. Third radiation transfer model intercomparison (RAMI) exercise: documenting progress in canopy reflectance models. J. Geophys. Res. 112, D09111.

Widlowski, J.L., Mio, C., Disney, M., Adams, J., Andredakis, I., Atzberger, C., Brennan, J., Busetto, L., Chelle, M., Ceccherini, G., Colombo, R., Côté, J.F., Eenmäe, A., Essery, R., Gastellu-Etchegorry, J.P., Gobron, N., Grau, E., Haverd, V., Homolová, L., Huang, H., Hunt, L., Kobayashi, H., Koetz, B., Kuusk, A., Kuusk, J., Lang, M., Lewis, P.E., Lovell, J., Malenovský, Z., Meroni, M., Morsdorf, F., Möttus, M., Ni-Meister, W., Pinty, B., Rautiainen, M., Schlerf, M., Somers, B., Stuckens, J., Verstraete, M.M., Yang, W., Zhao, F., Zenone, T., 2015. The fourth phase of the radiative transfer model intercomparison (RAMI) exercise. Actual canopy scenarios and conformity testing. Remote Sens. Environ. 169, 418–437.

Wilkes, P., Lau, A., Disney, M., Calders, K., Burt, A., de Tanago, J.G., Bartholomeus, H., Brede, B., Herold, M., 2017. Data acquisition considerations for terrestrial laser scanning of forest plots. Remote Sens. Environ. 196, 140–153.

WMO, 2012. Requirements Defined for Leaf Area Index (LAI). Available on http://www.wmo-sat.info/oscar/variables/view/98.

Woodgate, W., Soto-Berelov, M., Suarez, L., Jones, S., Hill, M., Wilkes, P., Axelsson, C., Haywood, A., Mellor, A., 2012. Searching for the optimal sampling design for measuring LAI in an upland rainforest. In: Proceedings of the Geospatial Science Research Symposium GSR2. December 2012, Melbourne.

Woodgate, W., Disney, M., Armston, J.D., Jones, S.D., Suarez, L., Hill, M.J., Wilkes, P., Soto-Berelov, M., Haywood, A., Mellor, A., 2015a. An improved theoretical model of canopy gap probability for leaf area index estimation in woody ecosystems. For. Ecol. Manag. 358, 303–320.

Woodgate, W., Jones, S.D., Suarez, L., Hill, M.J., Armston, J.D., Wilkes, P., Soto-Berelov, M., Haywood, A., Mellor, A., 2015b. Understanding the variability in ground-based methods for retrieving canopy openness, gap fraction, and leaf area index in diverse forest systems. Agric. For. Meteorol. 205, 83–95.

Woodgate, W., Armston, J., Disney, M., Jones, S., Suarez, L., Hill, M., Wilkes, P., Soto-Berelov, M., 2016. Quantifying the impact of woody material on leaf area index estimation from hemispherical photography using 3D canopy simulations. Agric. For. Meteorol. 226–227, 1–12.

Woodgate, W., Armston, J., Disney, M., Suarez, L., Jones, M., Hill, S., Wilkes, M., Soto-Berelov, P.M., 2017. Validating canopy clumping retrieval methods using hemispherical photography in a simulated eucalypt forest. Agric. For. Meteorol. 247, 181–193.

Zhao, F., Yang, X., Schull, M.A., Román-Colón, M.O., Yao, T., Wang, Z., Zhang, Q., Jupp, D.L.B., Lovell, J.L., Culvenor, D.S., Newnham, G.J., Richardson, A.D., Ni-Meister, W., Schaaf, C.L., Woodcock, C.E., et al., 2011. Measuring effective leaf area index, foliage profile, and stand height in New England forest stands using a full-waveform ground-based LiDAR. Remote Sens. Environ. 115, 2954–2964.